Ionic Liquids

DOI: 10.1002/anie.200900300

Double Layer of Au(100)/Ionic Liquid Interface and Its Stability in Imidazolium-Based Ionic Liquids**

*Yu-Zhuan Su, Yong-Chun Fu, Jia-Wei Yan, Zhao-Bin Chen, and Bing-Wei Mao**

Non-chloroaluminated room-temperature ionic liquids (RTILs) have received increasing attention in recent years as a new type of organic reaction medium because of their broad applications in various fields, such as catalysis, electrochemistry, and (bio)analysis.[1] Electrochemistry benefits mostly from the wide electrochemical window, high conductivity, and vanishingly low vapor pressure of the ionic liquids.[2] These features not only facilitate investigations into metal electrodeposition,[3] electrocapacitors,[4] and electrocatalysis[5] in a less demanding manner, but also open up new possibilities for increased reactivity of processes and/or stability of reactants/products in ionic liquids. However, organic cations of the ionic liquids may interact with electrode surfaces. It has been observed by using in situ scanning tunneling microscopy (STM) that bare Au(111) electrode surfaces encounter a long-range restructuring in ionic liquids consisting of imidazolium-type cations as a result of increasing interaction with the cationic imidazolium in a certain potential region.[6] Such an interaction could have an undesirable impact on the electrode processes as well as other heterogeneous processes in ionic liquids. Understanding the structures and properties of solvent ionic liquids at electrified interfaces is important before they can be truly regarded as inert solvents for various applications.[7]

Theories about the electric double layer at complex electrode/ionic liquid interfaces are emerging.[8–10] For example, Kornyshev first derived a new analytical formula based on the statistical mechanics of a dense Coulomb system at a planar metal/ionic liquid interface, assuming the absence of specific adsorption of ions.[8,10] By introducing a γ factor, which denotes the degree of lattice saturation of ions, a bell-shaped potential dependence of differential capacitance is predicted for ionic liquids with a capacitance maximum or local minimum close to the potential of zero charge (PZC) of the system, depending on the size symmetry of the cations and anions of the liquids.[8,10] A camel-shaped potential dependence of capacitance is also predicted under conditions with $\gamma < 1/3$. Experimental approaches have also been reported on differential capacitance measurements[11–13] as well as in situ spectroscopic characterizations[14–16] in ionic liquids by employing polycrystalline electrodes. Parabolic,[11] bell-shaped,[12] or camel-shaped[13] differential capacitance curves have been observed, and focus is given to correlating the PZC with capacitance maximum or minimum. Results from in situ sum frequency generation (SFG),[14] surface-enhanced Raman spectroscopy (SERS),[15] Fourier transform IR adsorption spectroscopy (FTIRAS), and surface-enhanced IR adsorption spectroscopy (SEIRAS)[16] suggest an orientation change of the imidazolium ring from a flat to a vertical configuration at the surfaces of Pt, Ag, and Au electrodes as their potentials are made less negative.

However, the employment of polycrystalline electrodes in the above-mentioned studies adds complexities for precise analysis and theoretical modeling. More importantly, there is a lack of long-range order of ionic adsorption on such polycrystalline surfaces, which could otherwise contain rich information about the interaction of ionic liquids with surfaces. Undoubtedly the employment of well-defined single-crystal surfaces is crucial for further comprehensive understanding of the adsorption behavior of imidazolium cations at electrified interfaces from a structural point of view. Unfortunately, direct molecular-resolution characterization of the cationic adsorption of ionic liquids by structurally sensitive in situ STM has not been achieved up to now. This situation hinders the provision of a clear microscopic picture of the metal/ionic liquid interfaces.

Herein, we report the double-layer behavior of Au(100) in ionic liquids that consist of 1-butyl-3-methylimidazolium cations (BMI^+) and BF_4^- or PF_6^- anions. We show that the differential capacitance curves of the systems have a bell-shaped feature and that BMI^+ adsorption at Au single-crystal electrodes depends critically on the structure of the surfaces.

Descriptions of the experimental procedures used for electrochemical and in situ STM measurements are given as Supporting Information. Au(100) in $[BMI]BF_4$ has an apparent electrochemical window of up to ≈ 4.0 V[17] with negligible current in a wide potential region between -2.3 and 1.6 V (Supporting Information, Figure S1). Starting from the initial potential at -0.3 V, cathodic and anodic potential excursion was applied in the double-layer region and the differential capacitance was measured as a function of potential. As shown in Figure 1, the capacitance versus potential curve displays an asymmetric bell-shaped feature with a notable peak of 27 $\mu F\,cm^{-2}$ at around -0.6 V, and the positive wing in region A is higher than the negative one in region C. Note also the subtle changes in the middle part of region B in Figure 1, marked by a dotted oval. These features are

[*] Y.-Z. Su, Y.-C. Fu, Dr. J.-W. Yan, Z.-B. Chen, Prof. Dr. B.-W. Mao
State Key Laboratory of Physical Chemistry of Solid Surfaces and Department of Chemistry, College of Chemistry and Chemical Engineering, Xiamen University, Xiamen 361005 (China)
Fax: (+86) 592-2183047
E-mail: bwmao@xmu.edu.cn

[**] We gratefully acknowledge valuable discussions with D.-Y. Wu, Y.-F. Huang, and S. Duan at Xiamen University. This work was supported by the Natural Science Foundation of China (Nos. 20433040, 20273056) and the National Basic Research Program of China (973 Program; 2007CB935603).

Supporting information for this article is available on the WWW under http://dx.doi.org/10.1002/anie.200900300.

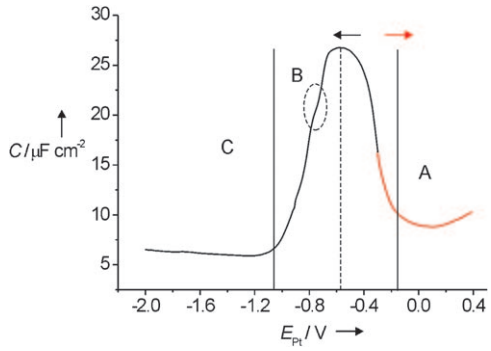

Figure 1. Differential capacitance (*C*) versus potential (*E*) curve of Au(100) in neat [BMI]BF_4 ionic liquid. As indicated by the two opposite arrows, the measurements were made anodically and cathodically from the same initial potential at −0.3 V. An ac modulation signal with $V_{p\text{-}p}=5$ mV and $f=18$ Hz was superimposed.

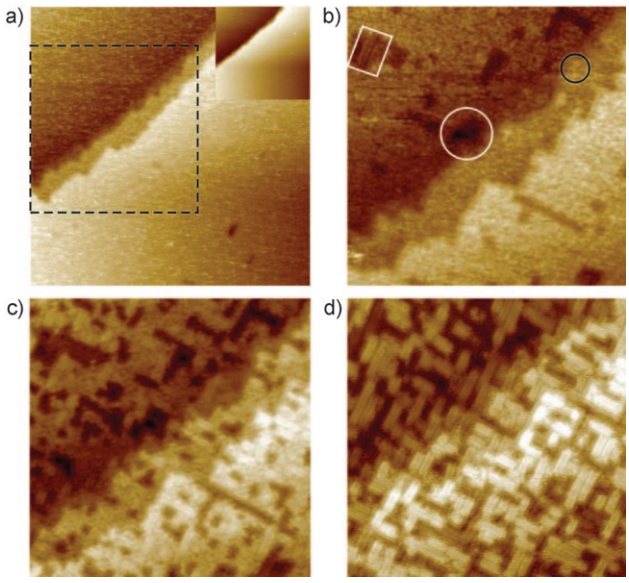

Figure 2. Sequence of STM images of Au(100) in [BMI]BF_4 showing adsorption of BMI^+ cations: a) −0.7 V; 15 min after (a) at b) −0.7, c) −0.8, and d) −0.95 V. The inset of (a) shows the bare surface of Au(100) at −0.65 V. Images (b–d) show the zoomed area marked by the dashed square in (a). Scan size: a) 100×100, b–d) 60×60 nm^2.

generally in agreement with Kornyshev's molecular dynamics simulation results for asymmetric ion size with the cations twice as large as the anions.[10b] We should mention that upon cathodic potential excursion to the negative potential region (<-1.2 V), which would induce surface reconstruction (see below), the capacitance curve does not show obvious changes but a near-flat plateau with a slight increase along with the potential decrease.

It is reasonable to expect that structural alteration of the interface would be significant across the capacitance maximum if the maximum is connected with adsorption/desorption of ions close to the PZC. To obtain a general idea about the surface structure associated with the capacitance features, in situ STM measurements were performed in the full range of potential within the electrochemical window. Starting from an unreconstructed Au(100) (1×1) surface at −0.3 V, an anodic potential excursion was applied first. The adsorption of BF_4^- occurs at potentials positive of −0.1 V (up to 0.4 V) in the form of an ordered $\begin{pmatrix} 3 & -1 \\ -1 & 3 \end{pmatrix}$ structure (see the Supporting Information). This feature is similar to that of PF_6^- adsorption on Au(111) in [BMI]PF_6,[18] except that PF_6^- forms a $(\sqrt{3}\times\sqrt{3})$ structure. Then, a cathodic potential excursion was applied starting from the same initial potential. An apparently clean bare surface is observed at −0.65 V, which is just around the capacitance maximum (see inset of Figure 2a), thus indicating a stage that is without immobilized adsorption of both anions and cations. Further decreasing the potential to −0.7 V, which is at the cathodic side of the capacitance maximum, leads to the formation of a loose filmlike layer which is attributed to disordered adsorption of BMI^+ cations (Figure 2a). Thus, the maximum of the bell-shaped capacitance curve implies a potential region of transition from anion adsorption to cation adsorption.

The filmlike disordered adsorption of BMI^+ leads to surface etching, which almost immediately generates surface defects within the BMI^+ film as well as in the underlying substrate surface, as indicated by the white square and circle, respectively, in Figure 2b. The square-marked defects are stable double-row strips with corrugation height of ≈0.05 nm, and the circle-marked defects are unstable holes up to two monolayers in depth, which develop along with time and potential. A few small islands are also observed, such as that indicated by the black circle in Figure 2b. Importantly, the disordered filmlike layer gradually fragments into anisotropic domains while creating more double-row strips within the domains (Figure 2c). Meanwhile, the holes between the domains are enlarged to expose the next layer of the surface. This surface-etching process has been verified by the increased atomic content of gold in the ionic liquid measured after experiments (Supporting Information, Table S1). However, the surface stabilizes at −0.95 V once all disordered parts of the domains turn into clear and perpendicularly oriented characteristic double-row strips (Figure 2d). We recognize the transition from the filmlike layer to the double-row strips as disorder–order transition of BMI^+ adsorption.

The clear STM image given in Figure 3a discloses some details of the strip structure. Each row of the strip is composed of aligned BMI^+ cations, with the large and bright spots being the imidazolium groups (or heads) and the less intense parts being the butyl side chains (or tails). The nearest-neighbor distance of head groups from the same row is (0.42 ± 0.02) nm, which is close to the lattice distance at the $\sqrt{2}$ direction of the unit cell of the Au(100) surface. The double rows are arranged in a tail-to-tail manner with either zigzag or straight-facing configuration. The length of the strips can vary from 3 to 30 nm depending on the experimental conditions (see the Supporting Information). The end of the double-row strip is closed, although frizzy (see the circles in Figure 3a and the Supporting Information, Figure S4), and we denote such a structure as a micelle-like structure. Both the zigzag-configured and straight-facing-configured micelle-like structures have a perpendicular head-to-head distance of (1.23 ± 0.02) nm. Based on this analysis, a structural model is

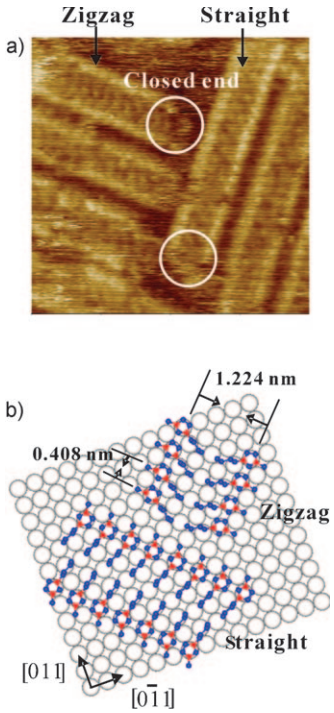

Figure 3. a) High-resolution STM image of BMI^+ adsorption from $[BMI]PF_6$ on Au(100) at −1.0 V. Scan size: 8×8 nm^2. b) Proposed model of BMI^+ adsorption structure.

proposed as shown in Figure 3b. In the model, the double rows lie along the two $\sqrt{2}$ directions of the Au(100) surface with the BMI^+ rings at the atop sites, although the exact positional alignment cannot be resolved based on the present available data. In addition, the zigzag-configured micelle-like structure has a mirror symmetry between the two rows and is thus of chiral character. The alignment of BMI^+ cations within the row and the tail-to-tail arrangement between the rows provides the most efficient configurations for interactions among the BMI^+ cations, which facilitates strong van der Waals interaction between the alkyl side chains and thus stabilizes the micelle-like structures.

It has been understood that aromatic and unsaturated organic compounds have the tendency to interact with metals (e.g., Au, Hg) through their π electrons.[13,19] The micelle-like adsorption of BMI^+ at a negatively charged surface is explained as fulfilled through coulombic forces as well as π-electron interactions. Both factors favor a parallel orientation of the BMI^+ rings relative to the surface. However, the final orientation has to be under crystallographic constraint in a limited space. It is likely, therefore, that the BMI^+ rings take a near-parallel orientation, with a slight incline, with respect to the surface. Spectroscopic data also support such a near-parallel orientation of the BMI^+ rings at a negatively charged surface.[14–16]

The micelle-like adsorption of the BMI^+ cations can be observed by employing different anions, such as PF_6^- and $SO_3CF_3^-$. However, the cation absorption only appears on the Au(100) surface, not on the Au(111) surface. Such a selective and ordered adsorption of BMI^+ on the Au(100) surface reveals the necessity of structural commensurability of the adsorbed BMI^+ with the surface. Nevertheless, the size of the BMI^+–Au(100) interaction is clearly lessened to an extent that is insufficient to etch the surface. This explains why a stable surface is reached upon completion of the disorder–order transition of the BMI^+ adsorption. In addition, the height of the strips measured with respect to the next layer of the strips is monoatomic ($\approx$0.2 nm), and therefore the strips are most likely composed of adsorbed BMI^+ cations on top of Au islands. Accordingly, the Au islands underneath the micelle-like structure would be against the surface etching.

The selective adsorption of BMI^+ on the Au(100) surface and the presence of Au islands right underneath the micelle-like structure are further proved by the change of surface morphology upon surface reconstruction from Au(100)(1×1) to the Au(100)-hex structure. The surface reconstruction initiates when the potential is decreased to −1.25 V, as can be identified by the appearance of reconstruction rows (indicated by arrows in Figure 4a), the orientation of which

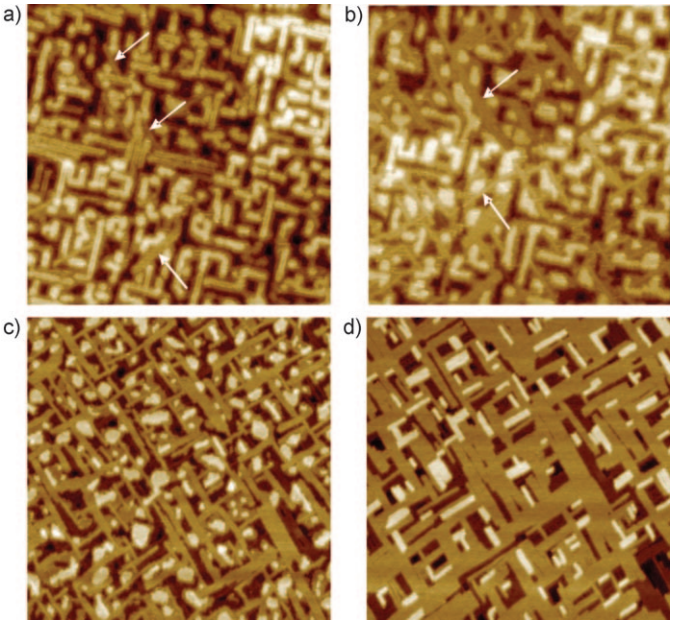

Figure 4. Sequence of STM images of Au(100) in $[BMI]BF_4$ showing the occurrence and progress of Au(100)-hex reconstruction at −1.25 V for a) 5, b) 8, and c) 40 min and at d) −2.3 V. Scan size: a,b): 100×100, c,d): 150×150 nm^2. Arrows indicate the reconstruction rows.

deviates from that of the double-row strips by 45°. Gradually, the original double-row strips change into round-shaped islands with loss of the strip feature along the $\sqrt{2}$ directions (Figure 4b and c). Eventually, a clear Au(100)-hex reconstructed surface is reached at sufficiently negative potential and with the consumption of some islands (Figure 4d), which is the same characteristic as in aqueous solutions.[20] Under these circumstances, the ordered micelle-like structure of BMI^+ adsorption cannot be maintained any more because of the unfavorable hexagonal arrangement of the reconstructed Au(100)-hex surface, as in the case of Au(111).[6] However, removal of the ordered micelle-like structure of BMI^+ adsorption does not lead to re-etching of the surface. One

of the reasons for this is that when the Au surface is of sufficiently negative charge density, the Au–Au bonding of the surface atoms is strengthened against etching by the adsorptive BMI^+ cations.

Summarizing the STM results, the molecular-resolution images of both BF_4^- and BMI^+ adsorption at unreconstructed Au(100)(1×1) are obtained. The adsorption of BMI^+ cations follows a potential-promoted disorder–order transition at the cathodic side of the capacitance maximum. The disordered adsorption of BMI^+ is dynamic and leads to surface etching, whereas the micelle-like arrangement of ordered adsorption of BMI^+ accommodates the ions with more efficient intermolecular interactions and prevents the surface from further etching. These processes are schematically illustrated in Figure 5.

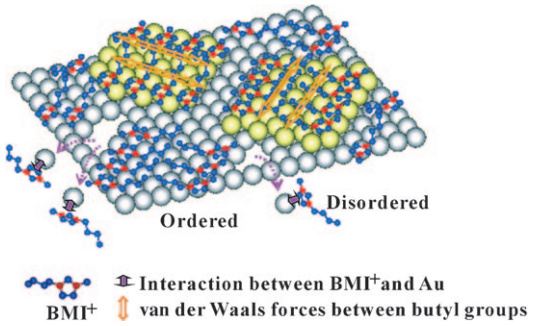

Figure 5. Schematic illustration of interactions of BMI^+ with the Au(100) surface. Strong interaction with dynamic disordered adsorption etches the surface, whereas weak interaction with ordered micelle-like adsorption stabilizes the surface.

In conclusion, we have performed a comprehensive investigation of the electrified Au(100) surfaces in RTILs by combined in situ STM and differential capacitance measurements. This serves as the first study that clearly correlates the capacitance features with the adsorption of ions of solvent ionic liquids on single-crystal electrodes. Furthermore, it has been revealed that the imidazolium-based cations may interact with the Au surfaces destructively. The transition from an absence of ordered adsorption of the imidazolium cations on hexagonally arranged Au surfaces, either Au(111)-(1×1)[6] or Au(100)-hex surfaces, to ordered micelle-like adsorption on the Au(100)(1×1) surface reveals a strong crystallographic dependency of the molecule–surface interaction. Such information is important to elucidate the role of molecule–surface and molecule–molecule interactions and provides a basis for reaching a clear physical picture about such interfaces. Equally important is the layout of the problems associated with the surface etching of the Au electrodes in a certain potential region. It is noted, however, that information about the surface etching seems not to be reflected by the differential capacitance curves, and safe and precise conclusions about double-layer structure can only be reached with proofs from other techniques, such as the structurally sensitive STM. Therefore, cautionary application of ionic liquids is necessary, especially for systems involving surface-sensitive processes. Further experimental and theoretical investigations employing different-natured cations are highly desirable for a thorough understanding of the role of cations of RTILs in electrochemical processes. Research towards this direction is currently under way in our laboratory.

Received: January 17, 2009
Revised: March 12, 2009
Published online: June 12, 2009

Keywords: adsorption · electrochemistry · ionic liquids · scanning probe microscopy · surface chemistry

[1] a) T. Welton, *Chem. Rev.* **1999**, *99*, 2071–2083; b) P. Wasserscheid, W. Keim, *Angew. Chem.* **2000**, *112*, 3926–3945; *Angew. Chem. Int. Ed.* **2000**, *39*, 3772–3789; c) M. Galinski, A. Lewandowski, I. Stepniak, *Electrochim. Acta* **2006**, *51*, 5567–5580; d) P. Domínguez de María, *Angew. Chem.* **2008**, *120*, 7066–7075; *Angew. Chem. Int. Ed.* **2008**, *47*, 6960–6968.
[2] M. C. Buzzeo, R. G. Evans, R. G. Compton, *ChemPhysChem* **2004**, *5*, 1106–1120.
[3] a) A. P. Abbott, K. J. McKenzie, *Phys. Chem. Chem. Phys.* **2006**, *8*, 4265–4279; b) F. Endres, M. Bukowski, R. Hempelmann, H. Natter, *Angew. Chem.* **2003**, *115*, 3550–3552; *Angew. Chem. Int. Ed.* **2003**, *42*, 3428–3430.
[4] a) A. Lewandowski, A. Swiderska, *Solid State Ionics* **2003**, *161*, 243–249; b) Q. Zhu, Y. Song, X.-F. Zhu, X.-L. Wang, *J. Electroanal. Chem.* **2007**, *601*, 229–236.
[5] a) S.-F. Wang, T. Chen, Z.-L. Zhang, X.-C. Shen, Z.-X. Lu, D.-W. Pang, K.-Y. Wong, *Langmuir* **2005**, *21*, 9260–9266; b) X.-B. Lu, J.-Q. Hu, X. Yao, Z.-P. Wang, J.-H. Li, *Biomacromolecules* **2006**, *7*, 975–980.
[6] L.-G. Lin, Y. Wang, J.-W. Yan, Y.-Z. Yuan, J. Xiang, B.-W. Mao, *Electrochem. Commun.* **2003**, *5*, 995–999.
[7] M. Mezger et al., see the Supporting Information.
[8] A. A. Kornyshev, *J. Phys. Chem. B* **2007**, *111*, 5545–5557.
[9] K. B. Oldham, *J. Electroanal. Chem.* **2008**, *613*, 131–138.
[10] a) M. V. Fedorov, A. A. Kornyshev, *Electrochim. Acta* **2008**, *53*, 6835–6840; b) M. V. Fedorov, A. A. Kornyshev, *J. Phys. Chem. B* **2008**, *112*, 11868–11872.
[11] a) M. T. Alam, M. M. Islam, T. Okajima, T. Ohsaka, *Electrochem. Commun.* **2007**, *9*, 2370–2374; b) M. T. Alam, M. M. Islam, T. Okajima, T. Ohsaka, *J. Phys. Chem. C* **2008**, *112*, 2601–2606.
[12] M. M. Islam, M. T. Alam, T. Ohsaka, *J. Phys. Chem. C* **2008**, *112*, 16568–16574.
[13] V. Lockett, R. Sedev, J. Ralston, M. Horne, T. Rodopoulos, *J. Phys. Chem. B* **2008**, *112*, 7486–7495.
[14] a) S. Rivera-Rubero, S. Baldelli, *J. Phys. Chem. B* **2004**, *108*, 15133–15140; b) S. Baldelli, *J. Phys. Chem. B* **2005**, *109*, 13049–13051.
[15] V. O. Santos, M. B. Alves, M. S. Carvalho, P. A. Z. Suarez, J. C. Rubim, *J. Phys. Chem. B* **2006**, *110*, 20379–20385.
[16] a) N. Nanbu, Y. Sasaki, F. Kitamura, *Electrochem. Commun.* **2003**, *5*, 383–387; b) N. Nanbu, T. Kato, Y. Sasaki, F. Kitamura, *Electrochemistry* **2005**, *73*, 610–613.
[17] L. Xiao, K. E. Johnson, *J. Electrochem. Soc.* **2003**, *150*, E307.
[18] G.-B. Pan, W. Freyland, *Chem. Phys. Lett.* **2006**, *427*, 96–100.
[19] A. N. Frumkin, B. B. Damaskin in *Modern Aspects of Electrochemistry, Vol. 3* (Eds.: J. O'M. Bockris, B. E. Conway), Butterworth, London, **1964**, pp. 163–164.
[20] a) D. M. Kolb, *Angew. Chem.* **2001**, *113*, 1198–1220; *Angew. Chem. Int. Ed.* **2001**, *40*, 1162–1181; b) D. M. Kolb, J. Schneider, *Electrochim. Acta* **1986**, *31*, 929.

